Spatial scaling issues in constitutive modelling of geomaterials

†C.T. Nguyen¹, *G.D. Nguyen¹, H.H.Bui², and V.P. Nguyen¹

¹School of Civil, Environmental and Mining Engineering, University of Adelaide, Australia.

²Department of Civil Engineering, Monash University, Australia

*Presenting author: g.nguyen@adelaide.edu.au †Corresponding author: chi.nguyen@adelaide.edu.au

Abstract

Most geomaterials exhibit localised modes of failure, which appear in the form of shear bands or cracks. This appearance could be gradual or very abrupt, depending on the type of materials and also loading conditions. In particular, failure of rocks or concrete is very abrupt in tension and indicates the brittle nature of these materials under such conditions, while in compression regime and under increasing confining conditions, their failure gradually becomes more ductile with the onset and propagation of shear bands. The orientation and size of shear bands and/or fracture process zones in localised failure vary with the loading and materials. As a consequence, a correct description of geomaterial behaviour must take into account all these characteristics of failure. This is however not always the case in constitutive modelling of geomaterials, and while working well under homogeneous condition, most (if not all) existing models do not possess details on the size and orientation of localisation zones when localised failure takes place. This prevents them from capturing correctly the failure behaviour of the materials, the most important characteristic of which is size effect. We present in this study a new approach to incorporating both size and orientation of localisation zone in constitutive models for geomaterials. The concepts together with technical details, and preliminary results are presented to show the potentials of the new approach.

Keywords: Localisation, Size effects, Geomaterials, Constitutive Modelling

Introduction

Constitutive models play a key role in correctly predicting load carrying capacity and failure of materials and structures. They give a mathematical description of material behaviour under different loading conditions, and it is essential that this description follows closely the observed behaviour of materials in experiments and/or real life. This requires not only advanced experimental techniques for better understanding of material behaviour, but also a generic and strong theoretical framework to transfer this understanding to a constitutive model. In geomaterial modelling, while the experimental part has been advancing quickly in the last few decades, with sophisticated techniques such as X-Ray and Digital Image Correlation [Alshibli and Sture (1999); Desrues and Viggiani (2004), Réthoré et al (2007)] for the observation of failure initiation at the micro scale, in our opinion, the development of a theoretical framework to accommodate these experimental development is still lagging behind. Despite the developments of more and more advanced constitutive models, one of the most important features of geomaterial failure - localised failure mode and the associated size effect - is still an outstanding issue in constitutive models for geomaterials.

Localisation of deformation appears in the form of thin bands such as shear bands in soils or fracture process zones in concrete/rock under tensile loadings. The material outside a localisation band usually unloads elastically, giving the indication that most (or all) inelastic behaviour happens

inside this thin band. In addition, while the orientation of a localisation band depends on loading conditions [Runesson and Ottosen (1991)], the size and behaviour of the material inside this band are material characteristics. It can be seen that classical continuum models utilise a single stressstrain relationship under both diffuse and localised modes of failure; this is not adequate, due to lack of details on the size and behaviour of the localisation band to capture correctly localised failure of the material. A correct description of failure must, therefore, account for the transition from diffuse to localised mode, and the progression of material failure beyond that. In this sense, most existing models ignore localised failure and size effect issues, either partly or completely, in the model developments and interpretation/mapping of experimental data. In particular, they possess no details on the size, orientation and evolution of the localisation band. As a consequence, their behaviour does not scale with the volume, and hence size effects cannot be captured. This requires ad hoc treatments incorporated later, after the model development, should these models be used in the analysis of failure that involves numerical methods for the solutions of boundary value problems. Typical examples of these treatments are the nonlocal/gradient regularisation [Bažant and Lin (1988); de Borst and Muhlhaus (1992)], and viscous regularisation [Forest, E. Lorentz (2004)], with several corresponding applications in geomaterial modelling [Pedersen et al (2008); Nguyen and Einav (2010); Das et al (2013)]. Other examples to overcome deficiencies of existing continuum models in capturing localised failure and size effects involve enhancements to the discretisation techniques (e.g. finite element methods) to correctly describe the kinematics of localised failure and behaviour.

In this study, we start from a key characteristic of localisation in constitutive modelling of geomaterials: kinematics of localised failure, and enhancement is developed after enriching the kinematics of constitutive models. In this sense, an enriched constitutive model will possess more than one stress-strain relationships to correctly describe different material behaviours in- and outside the localisation zone. Size effects are automatically taken into account thanks to the intrinsic material length scale in the framework. A new formulation will be established and applied to different kinds of existing constitutive models. Numerical examples at the constitutive levels are used to illustrate key features of the new theoretical framework.

Kinematic enrichment at the constitutive level

Localised deformation takes place at certain stage of the deformation process (Fig. 1), with the onset and propagation of localisation band, where inelastic response occurs. This leads to incorrect representation of the deformation if a single homogeneous strain is used, as in classical continuum models (Fig. 2). In other words, the strain in the volume where constitutive model is defined is no longer homogeneous, while homogenised deformation is considered only appropriate inside the localisation zone and the bulk material outside it.

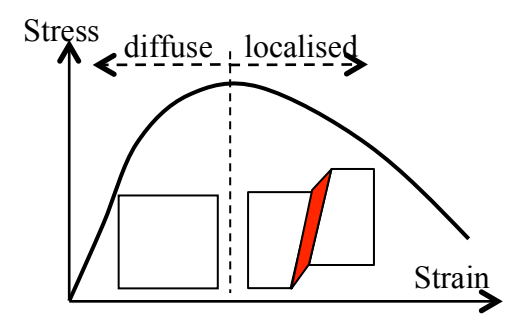


Figure 1. Diffuse and localised stages.

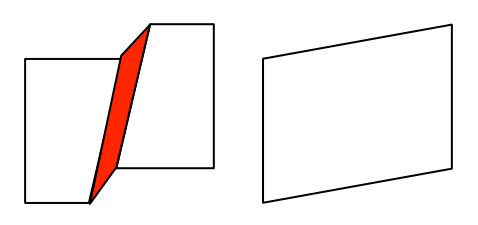


Figure 2. Observed localised failure and classical assumption of homogenous deformation.

In this section, the connection between the averaged (macro) stress σ and averaged (macro) strain ε over the domain Ω crossed by a localisation band (Figs. 1 & 2) is derived by coupling the response of the material inside and outside the localised region. For the volume of consideration, the stresses and strains for materials inside the localisation band and outside the homogeneous bulk are denoted as $(\sigma_i, \varepsilon_i)$ and $(\sigma_0, \varepsilon_0)$ respectively.

As can be seen in Fig. 2, two strain measures and correspondingly two stresses are required to capture correctly localised deformation, while for backward compatibility with existing numerical codes that takes a single stress-strain relationship, a macro stress-strain relationship is needed. For this, the macro strain rate is defined as the volume averaged quantity:

$$\dot{\boldsymbol{\varepsilon}} = f \dot{\boldsymbol{\varepsilon}}_i + (1 - f) \dot{\boldsymbol{\varepsilon}}_o \tag{1}$$

in which f, the volume fraction of the localisation zone, is defined as the ratio between the width h of the localisation zone and the effective size H of the volume element:

$$f = \frac{hA}{Q} = \frac{h}{H} \tag{2}$$

where A is the surface area of the localisation zone. The strain inside the localisation zone takes the following form (Nguyen et al, 2012):

$$\dot{\boldsymbol{\varepsilon}}_i = \frac{1}{h} (\boldsymbol{n} \otimes [\dot{\boldsymbol{u}}])^s \tag{3}$$

where n denotes the normal vector of the band and $[\dot{u}]$ is the relative velocity between opposite sides of the localisation band. We note that homogeneous term was ignored in the above equation, on the assumption that the deformation inside the localisation zone is usually of higher order of magnitude than that in the bulk volume containing it [Vardoulakis et al (1978), Vardoulakis and Graf (1985a; 1985b)]. This simplifies the formulation and also makes it adaptable to other cases of quasi-brittle modelling (Nguyen et al, 2014). The macro stress in this case cannot assume a volume averaged form, but needs to be worked out from the virtual work equation in the following form:

$$\boldsymbol{\sigma}: \dot{\boldsymbol{\varepsilon}} = f \boldsymbol{\sigma}_i: \dot{\boldsymbol{\varepsilon}}_i + (1 - f) \boldsymbol{\sigma}_o: \dot{\boldsymbol{\varepsilon}}_o$$
(4)

Substituting (1) and (3) into the above and after some rearrangement, we have:

$$\frac{f}{h}(\boldsymbol{t} - \boldsymbol{t}_i) \cdot [\dot{\boldsymbol{u}}] + (1 - f)(\boldsymbol{\sigma} - \boldsymbol{\sigma}_o) : \dot{\boldsymbol{\varepsilon}}_o = \boldsymbol{0}$$
 (5)

in which $t = \sigma \cdot n$ and $t_i = \sigma_i \cdot n$ are the tractions associated with the macro stress and the stress inside the localisation zone, respectively.

Since the strain rate and velocity jumps are arbitrary the following conditions are obtained:

$$\mathbf{t} = \mathbf{t}_i$$
, and $\mathbf{\sigma} = \mathbf{\sigma}_o$ (6a,b)

Given

$$\dot{\boldsymbol{\sigma}}_{0} = \mathbf{D}_{0} : \dot{\boldsymbol{\varepsilon}}_{0}, \text{ and } \dot{\boldsymbol{\sigma}}_{i} = \mathbf{D}_{i}^{T} : \dot{\boldsymbol{\varepsilon}}_{i}$$
 (7a,b)

as generic constitutive behaviours for the macro volume element and the localisation zone, with \mathbf{D}_o and \mathbf{D}_i^T being the corresponding tangent stiffnesses, using equations (1, 3, 6), we can solve for the velocity jump as:

$$[\dot{\boldsymbol{u}}] = \underbrace{\left[\frac{f}{h}(\boldsymbol{n} \cdot \boldsymbol{D}_o \cdot \boldsymbol{n}) + \frac{1-f}{h}(\boldsymbol{n} \cdot \boldsymbol{D}_i^T \cdot \boldsymbol{n})\right]^{-1}}_{C} \cdot (\boldsymbol{D}_o : \dot{\boldsymbol{\varepsilon}}) \cdot \boldsymbol{n}$$
(8)

Substituting (1, 3 and 8) into (7a) and rearranging the obtained expression, we get the macro stress-strain relationship in the rate form as:

$$\dot{\boldsymbol{\sigma}} = \frac{1 - f}{h} \boldsymbol{D}_o : \left\{ \dot{\boldsymbol{\varepsilon}} - \frac{1}{H} [\boldsymbol{n} \otimes (\boldsymbol{C}^{-1} \cdot (\boldsymbol{D}_o : \dot{\boldsymbol{\varepsilon}}) \cdot \boldsymbol{n})]^s \right\}$$
(9)

in which tensors $\mathbf{A}_o = \mathbf{n} \cdot \mathbf{D}_o \cdot \mathbf{n}$ and $\mathbf{A}_i = \mathbf{n} \cdot \mathbf{D}_i^T \cdot \mathbf{n}$ are the acoustic tensors associated with the tangent stiffness outside and inside the localisation band, respectively. Further details on the approach can be found in Nguyen et al (2012 & 2014).

Numerical implementation

As mentioned in the previous section, the enriched approach focuses on the post-localisation behaviour which means it is active only when localised failure has been detected. Bifurcation analysis, therefore, is of crucial importance and is presented in this section. Later, the implicit stress update algorithms for the enriched approach is given.

Onset and orientation of localisation band

The deformation behaviour of geomaterials under some specific circumstances can bifurcate from homogeneous to inhomogeneous localisation. There are several equivalent methods used for detecting that bifurcation point [Rudnicki and Rice (1975); Ottosen and Runesson (1991); Nielsen and Schreyer (1993)]. The loss of positive definiteness of the acoustic tensor is used in this paper as the indication of the onset of a localisation band. The normal vector **n** determines the orientation of the localisation band and also indicates the occurrence of the discontinuous bifurcation by the loss of positive definiteness of the acoustic tensor **A** associated with the tangent stiffness **D** [Schreyer and Nielsen (1996); Chambonet al. (2000)]:

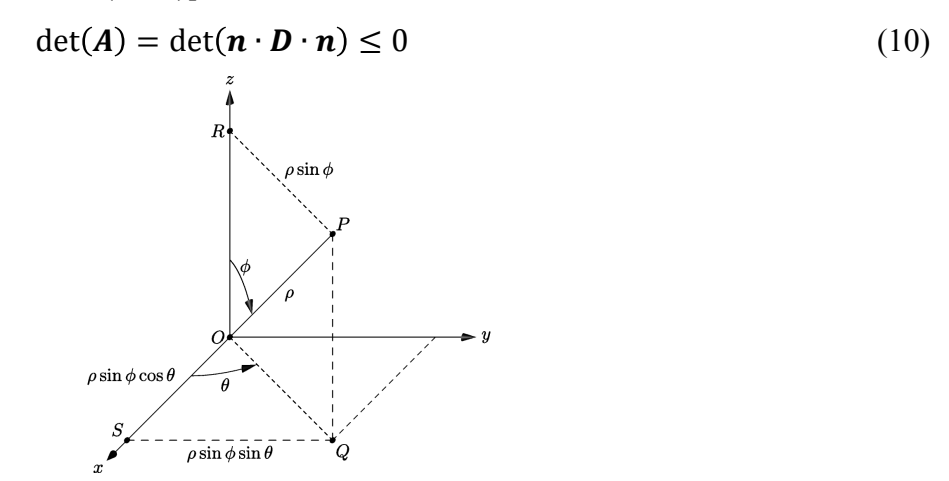


Figure 3. A spherical coordinates, after Wolfram

Using a standard spherical coordinates and define θ to be the azimuthal angle in the *xy*-plane from the *x*-axis with $0 \le \theta \le 2\pi$ and ϕ the zenith angle from the *z*-axis with $0 \le \phi \le \pi$, Fig. 3, the unit direction vector can be defined as following:

$$\boldsymbol{n} = \begin{bmatrix} n_x \\ n_y \\ n_z \end{bmatrix} = \begin{bmatrix} \sin \phi \cdot \cos \theta \\ \sin \phi \cdot \sin \theta \\ \cos \phi \end{bmatrix} \tag{11}$$

The matrix form of n, derived from the equation used to calculate the traction vector from the stress vector, is:

$$\boldsymbol{n} = \begin{bmatrix} n_x & 0 & 0 \\ 0 & n_y & 0 \\ 0 & 0 & n_z \\ n_y & n_x & 0 \\ 0 & n_z & n_y \\ n_z & 0 & n_x \end{bmatrix}$$
(12)

For the case of incrementally multi-linear models such as classical elasto-plastic models, a wide range of orientations can be physically admitted [Ottosen and Runesson (1991); Chambonet al. (2000)] hence it is determined through minimization of $\det(\mathbf{A})$ provided that $\det(\mathbf{A}) \leq 0$ [Sanborn and Prevost (2011)].

Implicit stress return algorithm

After the bifurcation point, a post-localisation analysis is performed with two distinct solutions of stresses and strains for the zones inside and outside the band. In this approach the macro stress coincides with the stress outside the localisation zone, whilst the macro strain is computed from the inside and outside strains and the volume fraction f. This section presents the stress update algorithm used in the enhanced approach.

Following the implicit algorithm, the traction equilibrium across the discontinuity plane is rewritten in the residual form as following:

$$r = \sigma \cdot \mathbf{n} - \sigma_i \cdot \mathbf{n} \tag{13}$$

then the iterative scheme is performed so that the norm of this residual is zero, indicating a converged solution in which the equilibrium across the discontinuity plane has been met. A first order Taylor expansion of the above equation at the state of the last iteration can be written as:

$$\mathbf{r}^{new} = \mathbf{r}^{old} + \delta \mathbf{\sigma} \cdot \mathbf{n} - \delta \mathbf{\sigma}_i \cdot \mathbf{n} \tag{14}$$

After some arrangement the following relation between the residual and the increment displacement jump is obtained:

$$\boldsymbol{r}^{new} = \boldsymbol{r}^{old} - \left[\frac{1}{1-f} \frac{f}{h} (\boldsymbol{n} \cdot \boldsymbol{D}_o \cdot \boldsymbol{n}) + \frac{1}{h} (\boldsymbol{n} \cdot \boldsymbol{D}_i^T \cdot \boldsymbol{n}) \right] \cdot \delta[\boldsymbol{u}]$$
(15)

Enforcing the requirement of $\mathbf{r}^{new} = 0$ leads to:

$$\delta[\mathbf{u}] = \left[\frac{1}{1-f}\mathbf{C}\right]^{-1} \cdot \mathbf{r}^{old} \tag{16}$$

Once $\delta[u]$ is calculated, the iterative strain inside the localisation band is computed as:

$$\delta \boldsymbol{\varepsilon}_i = \frac{1}{h} (\boldsymbol{n} \otimes \delta[\boldsymbol{u}])^s \tag{17}$$

then the stress increment $\delta \sigma_i$ is updated along with internal variables for the material inside the band and the tangent stiffness D_i . The convergence criteria is defined as:

$$\frac{\|r^{old}\|}{\|\sigma \cdot n\|} \le \text{TOLERANCE} \tag{18}$$

with TOLERANCE is a sufficiently small positive number.

A constitutive model based on breakage mechanics

The theoretical aspects and numerical implementation of the enriched approach are given in the previous sections. This section presents a specific constitutive model which will be used with the enriched approach to illustrate its capabilities. A breakage constitutive model [Einav (2007a)] is used to describe the behaviour of the material inside the localisation zone. First, a brief description of the breakage model is given including the stress-strain relationship, yield condition and tangent stiffness tensor; then performances of the model with and without using the enriched approach are given. For the shake of simplicity, the responses obtained without using the enriched approach are named "homogeneous", whereas the responses obtained using the enriched approach are named "localised" indicating that the localisation behaviour has been taken into account.

Model description

The breakage mechanics theory for crushable granular materials [Einav (2007a)] is built on the micromechanics of grains, using statistical homogenisation to upscale the grain-scale energy potential to obtain the macro energy potential of the continuum model. A simple breakage model proposed by Einav [2007b] and later improved by Nguyen and Einav [2009] is considered in this study. The following standard notations are used: bulk and shear modulus K and G, mean effective stress and deviatoric shear stress P and P0, total and elastic volumetric strain P1 and P2, total and elastic deviatoric shear strain P3 and P4, total and deviatoric stress tensor P6, and total, elastic and plastic strain tensors P6, and P7, the Kronecker delta P8, the Kronecker delta P9.

The stress-strain relationship in the triaxial stress space is:

$$p = (1 - \vartheta B) K \varepsilon_{\nu}^{e} \tag{19}$$

$$q = 3(1 - \vartheta B)G\varepsilon_s^e \tag{20}$$

The above relationships can also be written in tensorial form as:

$$\sigma_{ij} = (1 - \vartheta B) D_{ijkl} \varepsilon_{kl} \tag{19}$$

in which D_{ijkl} is the linear elastic stiffness tensor. The grading index θ is a result of the statistical homogenisation, and can be obtained from the initial and ultimate grain size distributions (gsd). Physically θ is related to the crushing potential of the materials and admits values from 0 to 1. The breakage variable B represents the degree of grain crushing, and is used to linearly interpolate the current gsd from the initial and ultimate gsd's [Einav, 2007a].

Einav [2007b] derived an elastic-plastic-breakage yield criterion, written in the mixed stress-breakage energy space as:

$$y_B = \frac{(1-B)^2 E_B}{E_C} + \left(\frac{q}{Mp}\right)^2 - 1 \le 0 \tag{22}$$

where M is the slope of the critical state line in the p-q space; E_C is the critical breakage energy which is computed from the critical crushing pressure during isotropic loading condition P_{cr} as:

$$E_C = \frac{P_{Cr}^2 \vartheta}{2K} \tag{23}$$

 E_B is the breakage energy, the thermodynamical conjugate to the breakage variable B, and has the form:

$$E_B = \frac{\vartheta}{2(1-\vartheta B)^2} \left(\frac{p^2}{K} + \frac{q^2}{3G}\right) \tag{23}$$

The evolution laws for the breakage and plastic strains can be written as:

$$dB = d\lambda \frac{2(1-B)^2 E_B \cos^2 \omega}{E_C}$$
 (24)

$$d\varepsilon_{ij}^p = d\lambda \left(-\frac{2(1-B)^2 E_B \sin^2 \omega}{p E_C} \frac{\delta_{ij}}{3} + \frac{3s_{ij}}{M^2 p^2} \right)$$
 (25)

in which $d\lambda$ is the nonnegative breakage/plasticity multiplier; ω is a parameter that couples the plastic volumetric deformation with grain crushing. Physically ω represents the pore collapse of the material due to grain crushing and reorganisation [Einav (2007a; 2007b)].

The incremental stress-strain relationship can be written as:

$$d\sigma_{ij} = L_{ijkl}d\varepsilon_{kl} \tag{26}$$

where the elastic-plastic-breakage tangent stiffness tensor L_{ijkl} has the form [Nguyen & Einav, 2009]:

$$L_{ijkl} = (1 - \vartheta B)D_{ijkl} - \frac{(1 - \vartheta B)X_{ij}Y_{mn}D_{mnkl}}{Y_{ij}X_{ij} - \frac{\partial y}{\partial B}}$$
(27)

in which:

$$X_{ij} = (1 - \vartheta B)D_{ijkl} \frac{\mathrm{d}\varepsilon_{ij}^p}{\mathrm{d}B} + \frac{\vartheta \sigma_{ij}}{1 - \vartheta B}$$
 (28)

$$Y_{ij} = \frac{\partial y}{\partial \sigma_{ij}} \tag{29}$$

Behaviour of the breakage model

For the illustration of the behaviour of the breakage model, a triaxial drained test simulation is performed at the constitutive level on the highly porous Bentheim sandstone. In the context of the triaxial test, the confining pressure p_0 means the initial isotropic confining pressure and this confining pressure is maintained horizontally during a strain-controlled axial loading.

Bentheim sandstone exhibits significant compactive behaviour and distinct compaction bands in experiments [Wong et al. (2001)]. Material parameters of Bentheim sandstone are taken from the reported experimental data and calibrated parameters [Wong et al. (2001), Das et al. (2011)]: bulk stiffness K = 138333 MPa, shear stiffness G = 7588 MPa, critical breakage energy $E_C = 4.67$ MPa, critical state parameter M = 1.7 MPa, grading index $\theta = 0.85$ and $\omega = 70^{\circ}$.

Fig. 4(a, b) presents the homogeneous responses of the breakage model in the drained triaxial test with different initial confining pressures. The increasing hardening of the breakage model is consistent with the experimental data [Baud et al (2004)] and represents the compactive cataclastic flow regime in which the stress-strain relationship is hardening and the porosity decrease monotonically with deformation [Wong et al. (2001)]. At the onset of inelastic deformation, localisation analysis is carried out following the classical bifurcation condition, Eq. (10-13). It is revealed that for all three confining pressures of 120, 180 and 240 MPa, bifurcation points exist and the corresponding inclination angles ϕ of the localisation surfaces are 35°, 15° and 0°, respectively.

Because of the symmetry in the triaxial loading condition, the angle θ (Fig. 3) is 90° in all three cases.

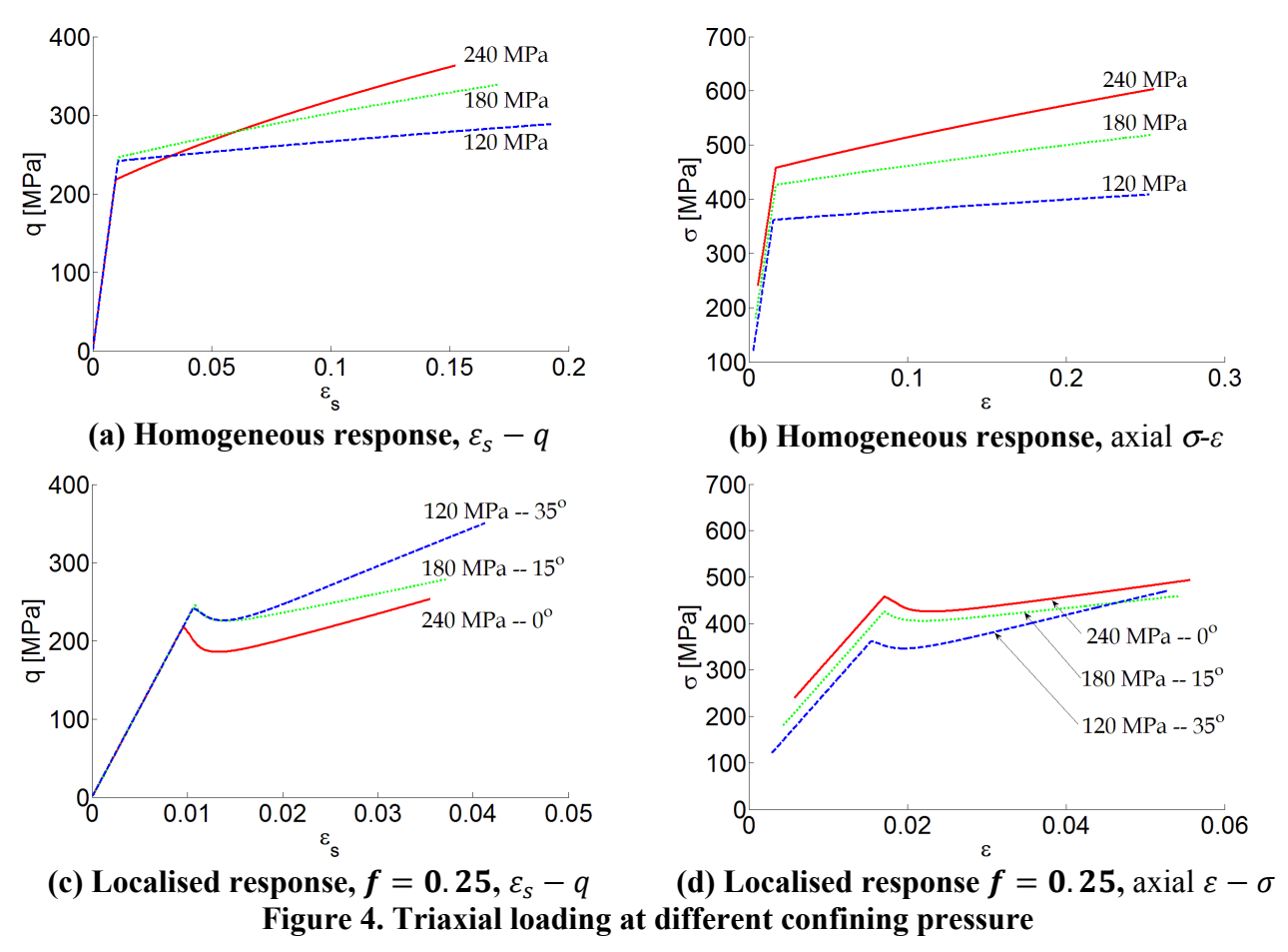
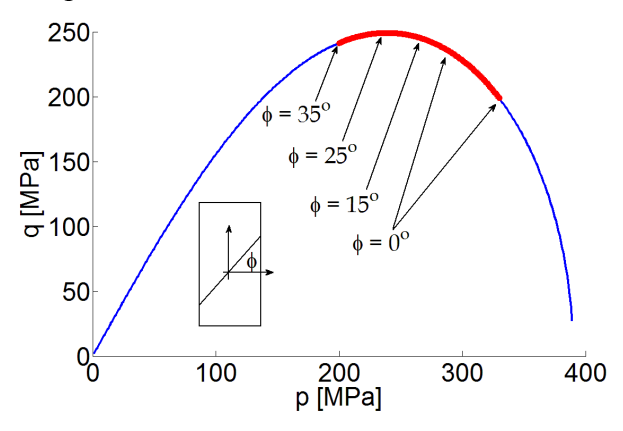


Fig. 4(c, d) depicts the localised responses following the enriched framework with the volume fraction f = h/H = 0.25 in the same loading conditions and given parameters. It is clear from Fig. 4 that localisation changes the material behaviour not only quantitatively but also qualitatively. The homogeneous behaviour is hardening but the localised behaviour, following the enriched framework, first exhibits softening associated with the activation and evolution of a localisation band, followed by hardening with the slope of the macro hardening much larger than that of the homogeneous hardening. Details of the localised behaviour are analysed in the next section.

Fig. 5 presents the initial yield envelopes obtained from the given constitutive parameters. The range of stress state along that initial yielding surface, in which the localisation bands most likely occur, is predicted numerically. In very high pressure regime, no localisation is observed which may be due to diffuse compaction band formation over the entire sample under high confining pressure [Wong et al. (2001)]. In such cases, the deformation may evolve into cataclastic flow without localisation [Das et al. (2011)]. However, as pointed out by Besuelle [2001], extension/dilation shear bands can form in Bentheim sandstone at low confining pressures. Note that the material behaviour at low confining pressures is not yet captured by this version of the breakage model. Fig. 5 also indicates that the inclination angle of the compact band varies from 0°-35° with the variation of the pressure regime, which implies that the localisation band is compactive dominant. In the high pressure regime, the angle is 0° which implies a pure compaction localisation

band; whereas in the medium pressure regime, the angle is about 30°-35° which implies a compactive shear localisation band.



 $\frac{1}{2}$ $\frac{1}$

Figure 5. Predicted zone of localisation

Figure 6. Contours of the determinant of the acoustic tensor

Fig. 6 presents the contours of the determinant of the acoustic tensor against the band orientation angle and the normalised mean stress (p/P_{cr} in which $P_{cr} = 389.87$ MPa) at the onset of crushing. In Fig. 6, the inner zone denotes negative determinant of the acoustic tensor which implies that localisation is possible only within this zone. It is clear from Fig. 6 that for a given stress state there is a set of inclination angles that are physically admissible in forming a localisation band. In the post-localisation analysis, only the angle with the minimum value of the determinant of the acoustic tensor is chosen as the inclination angle of the localisation band.

Size dependent behaviour

In this section, the performance of the enriched approach is investigated in details. The post-bifurcation responses of the Bentheim sandstone during the drained triaxial test are given in the first section; in the second section, the size dependent behaviour is proven by studying the influence of the localisation band width h on the macro responses.

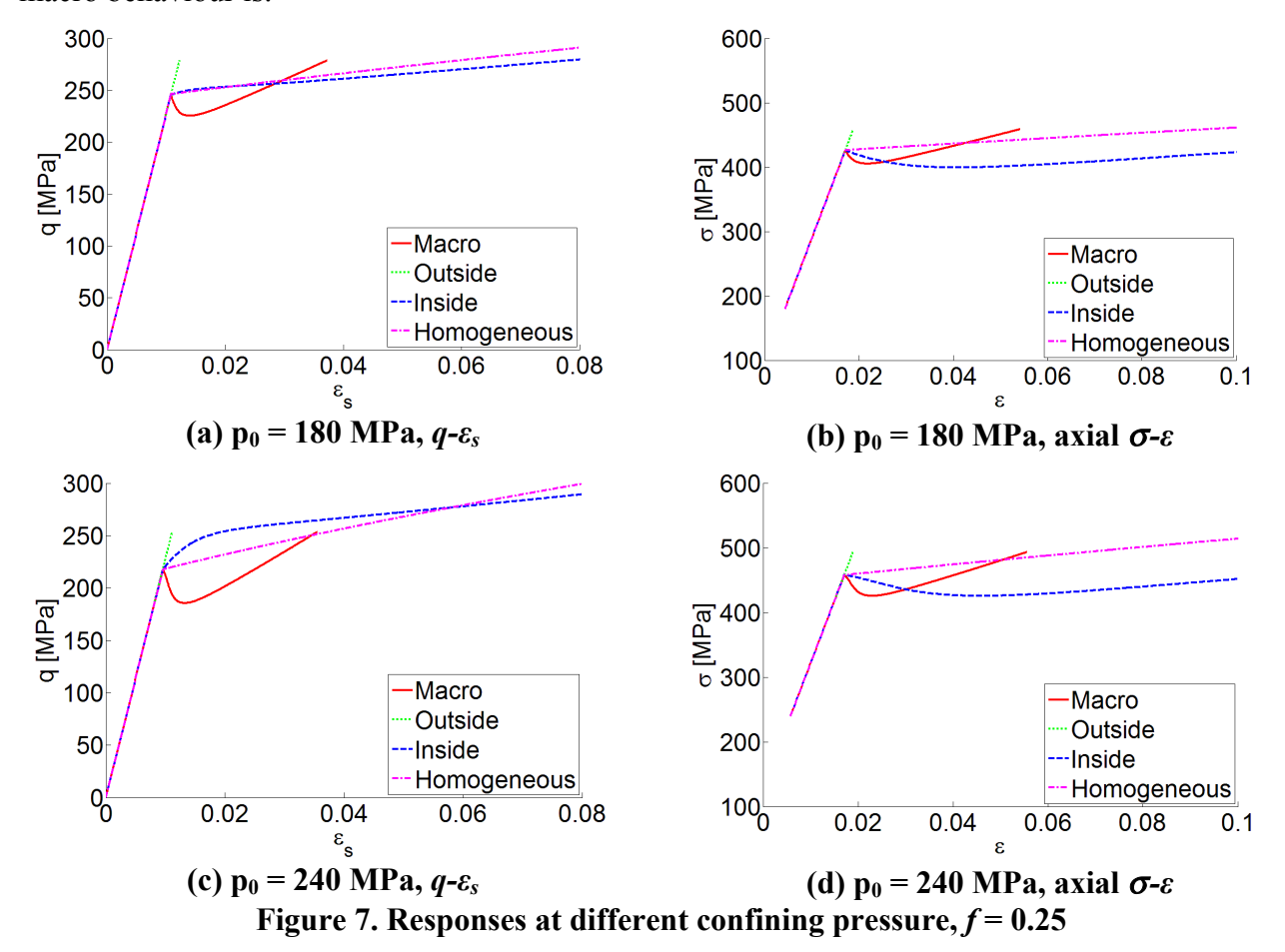
Post-bifurcation responses

The stress-strain responses during the drained triaxial test at different confining pressures obtained by using the enhanced framework are given in Fig. 7; the general responses $(q-\varepsilon_s)$ are given in Fig. 7(a, c) whereas the responses on the loading direction – in short: the axial response – $(\sigma-\varepsilon)$ are given in Fig. 7(b, d). Two confining pressures of 180 and 240 MPa, corresponding to two inclination angles of 15° and 35° of localisation bands, as calculated in the previous section from the bifurcation analysis, are applied. In these analyses, the volume fraction f is chosen to be 0.25.

It is clear from Fig. 7 that the general and axial homogeneous behaviours are always hardening whereas the macro localised behaviours are more complex. Initially after localisation, the mechanism of elastic unloading for the material outside the band and plastic hardening for the material inside the band dominates, leading to a steep softening behaviour for the macro material. However when the load reaches a minimum, the outside material starts behaving elastically, the macro softening terminates and the macro response is hardening. This hardening phase is then dominated and the localised hardening slope is much larger than the homogeneous hardening slope.

The general response of the material inside of the band is hardening with the long-term localised hardening slope is smaller than the homogeneous one, Fig. 7(a, c). This can be explained from the

fact that in the localised situation, only a band with the volume fraction f = 0.25 exhibit a hardening behaviour whereas in the homogeneous situation the whole sample is undergoing hardening deformation. It is also noted that the initial hardening slope in the localised response is larger with the larger confining pressure. This can originate from different types of the localisation bands at different confining pressures which changes from a compactive shear band, Fig. 7(a) with $\phi = 35^{\circ}$ to a pure compaction band, Fig. 7(c) with $\phi = 0^{\circ}$. On the loading direction, Fig. 7(b, d), the axial response of the inside material is first softening and then hardening which is analogous to how the macro behaviour is.



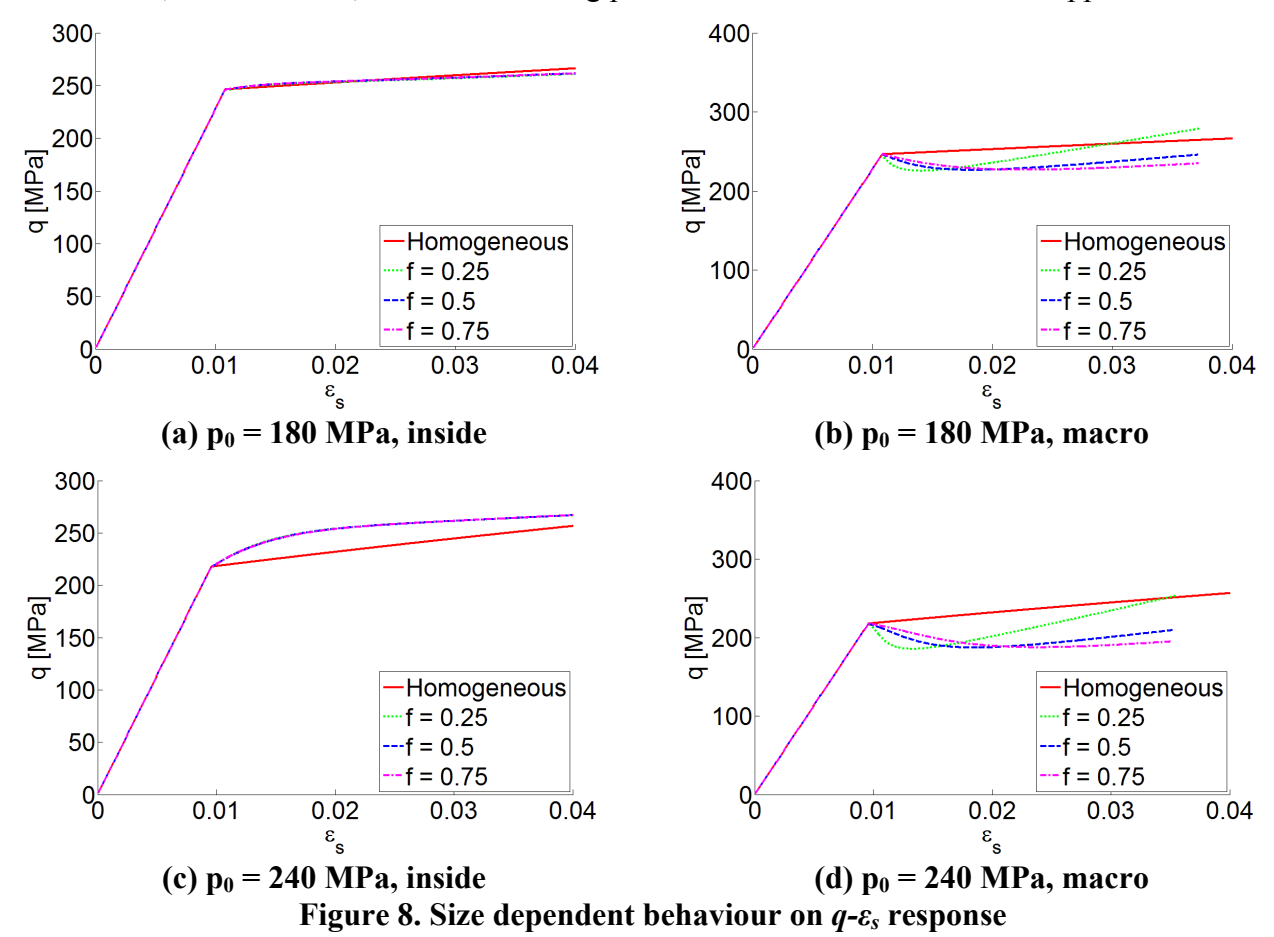
Since the homogeneous behaviour of the breakage model in drained triaxial tests is hardening, the initial strong softening behaviour originates from the kinematics enhancement occurred with strain localisation. Gajo et al [2004] also observed this saturation process and suggested that another mechanism of strain hardening is occurring inside the band, induced by the contractive behaviour of the material. It is worth mentioning that as the hardening phase is reached – or the band saturation process continues, at a certain point the material outside the localisation zone will reach the yield condition. At this point, a localised inelastic deformation occurs outside the band while the material inside the band starts elastic unloading, as suggested by Gajo et al [2004]. This behaviour is, however, not considered in this paper.

Effects of localisation band width

There is considerable experimental evidence on the relation between the shear band thickness h and the mean grain size d_{50} [Scarpelli and Wood (1982); Vardoulakis et al. (1985a; 1985b); Muhlhaus and Vardoulakis (1987)], usually given in the form:

$$h = (10 \div 15)d_{50} \tag{30}$$

This band width h is of a great importance in understanding and numerical modelling of progressive failure in granular materials [Gudehus (1978); Muhlhaus and Vardoulakis (1987)]. In this section, the size dependent behaviour in the drained triaxial test is investigated by varying the value of h whilst keeping H constant which means the volume fraction f is changed. Three values of f are chosen 0.25, 0.50 and 0.75, and two confining pressures of 180 and 240 MPa are applied.



It is clear from Fig. 8 (a, c) that the response of the material inside the localisation band is independent of the value of f. This independence implies that the macro dissipation energy, which only takes place inside the localisation band, scales linearly with the volume fraction of the band. Fig. 8 (b, d) illustrates that a size effect is exhibited since the macro response is strongly affected by the value of f. Since all of the dissipation energy occurs only inside the localisation band, apparently the smaller the value of f, the steeper the macro softening experiences initially. It can also be seen from Fig. 8 (b, d) that the band saturation process occurs at larger strain magnitude for the larger value of f which is explained by the fact that the localisation area is larger. Moreover, with a larger value of f, the influence of the elastically loading behaviour of the outside material on the subsequent hardening of the macro becomes smaller which is indicated by the smaller value of the hardening slope, Fig. 8 (b, d).

The experimental validation of the proposed constitutive model is shown in Fig. 9. The same set of parameters for the breakage model obtained from experimental data on Bentheim sandstone (see the preceding section on the breakage model) was used. A volume fraction f=0.35 needed for the enriched model was estimated from the experimental figures in [Baud et al (2004)]. We know that f

is evolving during failure of the material, so the fixed value of f=0.35 is used merely as a rough estimation to explore the trend of the material behaviour.

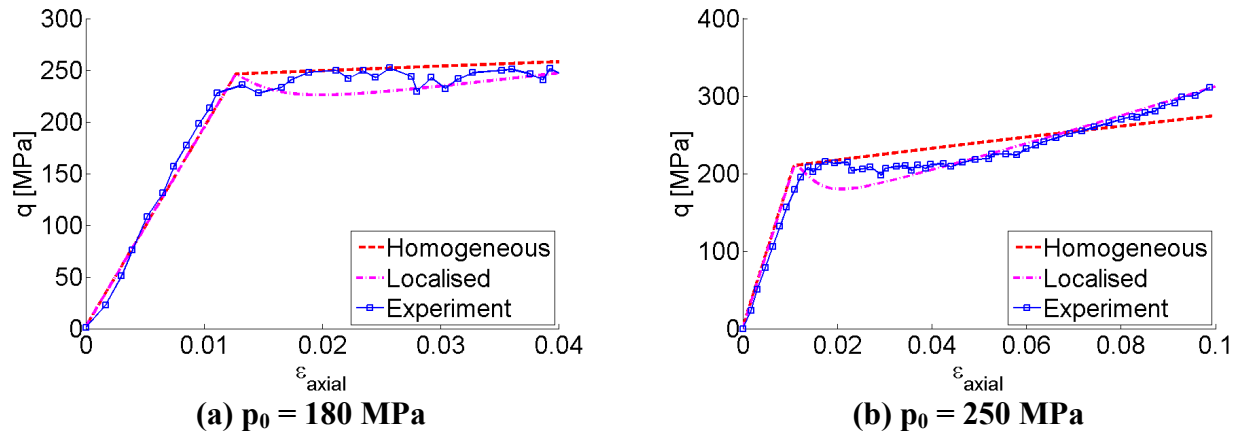


Figure 9. Validation of model response under different confining pressures

As can be seen in Fig. 9, the softening behaviour at the onset of localised failure, followed by hardening due to an increase of the density as a result of compaction, can be captured by the enriched model, while the original breakage model always exhibits a hardening trend. This preliminary result should serve as a basis for future improvements of the both the breakage model and the enrichment framework.

Conclusions

Theoretical development, numerical implementation and performance of a new constitutive modelling framework were presented in conjunction with the use of a model based on breakage mechanics for exploring localised failure in sandstone. The results explain the response of the material inside and outside the localisation band and how they influence the macro response. This helps improve both the performance and capacity of constitutive model in capturing post-bifurcation behaviour of geomaterials. Although the enriched approach provides a good understanding on the influence of the localised deformation, it is not adequate yet to capture correctly the material behaviour with oscillation in the macro response due to the gradual formation of several compaction bands during loading [Wong and Baud (2012); Das (2012)]. With that evolution of the localisation behaviour, inelastic behaviour outside the band must be also taken, and this is a subject of an on-going research.

Acknowledgements

Funding support from the Australian Research Council via projects DP110102645 and FT140100408 (Giang D. Nguyen) and LP13010088 (Ha Bui) is gratefully acknowledged.

Reference

- A. Das, G. Nguyen, I. Einav (2011), Compaction bands due to grain crushing in porous rocks: a theoretical approach based on breakage mechanics, *Journal of Geophysical Research* 116 1–14
- A. Das (2012), A theoretical study of grain crushing induced compaction localization in porous sandstones, PhDthesis University of Sydney
- A. Das, G. D. Nguyen, I. Einav (2013), The propagation of compaction bands in porous rocks based on breakagemechanics, *Journal of Geophysical Research: Solid Earth* 118 (5) 2049–2066
- A. Gajo, D. Bigoni and D. M. Wood (2004), Multiple shear band development and related instabilities in granular materials, *Journal of the mechanics and physics of solids* 52 2683-2724

- D. Kolymbas (1981), Bifurcation analysis for sand samples with a non-linear constitutive equation, *Ingenieur Archive* 50 (2) 31–40
- S. Forest, E. Lorentz (2004), Localization phenomena and regularization methods. *Local Approach to Fracture. Paris, Les Presses de l'Ecole des Mines* 311-371.
- G. D. Nguyen, I. Einav (2009), The energetics of cataclasis based on breakage mechanics, *Pure and AppliedGeophysics* 166 (10-11) 1693–1724
- G. D. Nguyen, I. Einav, A. M. Korsunsky (2012), How to connect two scales of behaviour in constitutive modelling of geomaterials, *Geotechnique Letters* 2, 129-134.
- G. D. Nguyen, A. M. Korsunsky, I. Einav (2014), A constitutive modelling framework featuring two scales of behaviour: Fundamentals and applications to quasi-brittle failure, *Engineering Fracture Mechanics* 115, 221–240.
- G.D. Nguyen, I. Einav (2010). Nonlocal regularisation of a model based on breakage mechanics for granular materials. *International Journal of Solids and Structures* 47(10) 1350-1360.
- G. Scarpelli, D.M. Wood (1982), Experimental observations of shear band patterns in direct shear tests. *Proc. IUTAM Conf. Deformation and Failure of Granular Materials, Delft* 473–484
- G. Gudehus (1978), Engineering approximations for some stability problems in geomechanics, *Advances in analysis of geotechnical instabilities, SM Study* 13 1–24
- H.-B. Muhlhaus, I. Vardoulakis (1987), The thickness of shear bands in granular materials, Geotechnique 37(3) 271-283
- H. Schreyer, M. Neilsen (1996), Analytical and numerical tests for loss of material stability, *International Journal for Numerical Methods in Engineering* 39 (10) 1721–1736.
- I. Einav (2007a), Breakage mechanics-part i: Theory, J Mech Physics Solids 55 (6) 1274 1297
- I. Einav (2007b), Breakage mechanics-part ii: Modelling granular materials, *J Mech Physics Solids* 55 (6) 1298 1320
- I. Vardoulakis, M. Goldscheider, G. Gudehus (1985a), Formation of shear bands in sand bodies as a bifurcation problem, *International journal of numerical and analytical methods in Geomechanics* 2 (0) (1978) 99–128
- I. Vardoulakis, B. Graf, Calibration of constitutive models for granular materials using data from biaxial experiments, *Geotechnique*35(3) 299–317
- I. Vardoulakis, B. Graf, A. Hettler (1985b), Shear band formation in a fine-grained sand, *Proc.* 5th Int. Conf. Numer. *Meth. Geomech.*, Nagoya1 517–521
- J. Desrues, G. Viggiani (2004), Strain localization in sand: an overview of the experimental results obtained in grenoble using stereophotogrammetry, International Journal for Numerical and Analytical Methods in Geomechanics 28 (4) 279–321.
- J. Rudnicki, J. Rice (1975), Conditions for the localization of deformation in pressure-sensitive dilatant materials, Journal of the Mechanics and Physics of Solids 23 (6) 371 – 394
- J. Rice (1976), The localization of plastic deformation, in: *Theoretical and Applied Mechanics, 14th IUTAM Congress*, North-Holland, Amsterdam
- J. Réthoré, F. Hild, S. Roux (2007), Shear-band capturing using a multiscale extended digital image correlation technique, Computer Methods in Applied Mechanics and Engineering, 196(49–52) 5016-5030
- K. Runesson, N. S. Ottosen, P. Dunja (1991), Discontinuous bifurcations of elastic-plastic solutions at plane stress and plane strain, International Journal of Plasticity 7 (1-2) 99–121.
- K. A. Alshibli, S. Sture (1999), Sand shear band thickness measurements by digital imaging techniques, Journal of Computing in Civil Engineering 13 (2) 103–109
- M. Neilsen, H. Schreyer (1993), Bifurcations in elastic-plastic materials, *International Journal of Solids and Structures* 30 (4) 521 544
- N. S. Ottosen, K. Runesson (1991), Properties of discontinuous bifurcation solutions in elasto-plasticity, *International Journal of Solids and Structures* 27 (4) 401 421
- P. Baud, E. Klein and T.-f. Wong (2004), Compaction localisation in porous sandstones: spatial evolution of damage and acoustic emission activity, Journal of Structural Geology, 26(2004), 603-624
- P. Besuelle (2001), Compacting and dilating shear bands in porous rocks: theoretical and experimental conditions, Journal of Geophysical Research 106 (-) 13435–13442
- P. Bažant, F.-B. Lin (1988), Non-local yield limit degradation, International Journal for Numerical Methods in Engineering 26 (8) 1805–1823.
- R. R. Pedersen, A. Simone, and L. J. Sluys (2008), An analysis of dynamic fracture in concrete with a continuum viscoelastic visco-plastic damage model. *Engineering Fracture Mechanics* 75(13) 3782-3805.
- R. de Borst, H.-B. Muhlhaus (1992), Gradient-dependent plasticity: Formulation and algorithmic aspects, *International Journal for Numerical Methods in Engineering* 35 (3) 521–539.
- R. Chambon, S. Crochepeyre, J. Desrues (2000), Localisation criteria for non-linear constitutive equations of geomaterials, *Mechanics of Cohesive-frictional Materials* 5 (-) 61–82
- S. Sanborn, J. Prevost (2011), Frictional slip plane growth by localisation detection and the extended finite element method (xfem), *International journal of numerical and analytical methods in Geomechanics* 35 (-) 1278–1298
- T.-f. Wong, P. Baud, and E. Klein (2001), Localised failure modes in a compactant porous rock, *Geophys. Res. Lett.*, 28(13), 2521–2524

T.-f. Wong and P. Baud (2012), The brittle-ductile transition in porous rock: A review, *Journal of structural geology*, 44, 25–53